Eur. Phys. J. Plus (2017) **132**: 112
DOI 10.1140/epjp/i2017-11369-0

THE EUROPEAN PHYSICAL JOURNAL PLUS

Regular Article

Modeling tangent hyperbolic nanoliquid flow with heat and mass flux conditions

T. Hayat[1,2], I. Ullah[1,a], A. Alsaedi[2], and B. Ahmad[2]

[1] Department of Mathematics, Quaid-I-Azam University 45320, Islamabad 44000, Pakistan
[2] NAAM: Research Group, Faculty of Science, King Abdulaziz University, P. O. Box 80207, Jeddah 21589, Saudi Arabia

Received: 20 December 2016
Published online: 3 March 2017 –

Abstract. This attempt predicts the hydromagnetic flow of a tangent hyperbolic nanofluid originated by a non-linear impermeable stretching surface. The considered nanofluid model takes into account the Brownian diffusion and thermophoresis characteristics. An incompressible liquid is electrically conducted in the presence of a non-uniformly applied magnetic field. Heat and mass transfer phenomena posses flux conditions. Mathematical formulation is developed by utilizing the boundary layer approach. A system of ordinary differential equations is obtained by employing adequate variables. Convergence for obtained series solutions is checked and explicitly verified through tables and plots. Effects of numerous pertinent variables on velocity, temperature and concentration fields are addressed. Computations for surface drag coefficient, heat transfer rate and mass transfer rate are presented and inspected for the influence of involved variables. Temperature is found to enhance for a higher magnetic variable. Present and previous outcomes in limiting sense are also compared.

1 Introduction

Investigation of non-Newtonian materials has relevance to many important applications. Especially such materials have remarkable involvement in oil reservoir engineering, geophysics, bioengineering, nuclear and chemical industries, cosmetic processes, polymer solution and many others. Few examples of non-Newtonian liquids include ketchup, slurries, certain oils and polymer solutions, paint, paper pulp, mud, shampoos and apple sauce. Clearly all non-Newtonian materials, because of their versatile behavior, cannot be predicted by a unique constitutive relationship. This concept distinguishes non-Newtonian and viscous liquids. Thus numerous models of non-Newtonian liquids are established in the literature to visualize the dynamics of such materials. For instance, the tangent hyperbolic liquid is a model capable to explore shear thinning characteristics, *i.e.*, its viscosity drops by an increment in shear rate. Peristalsis of hyperbolic tangent fluid in a non-uniform channel is studied by Abbas *et al.* [1]. Heat transfer flow of a hyperbolic tangent fluid flowing by a stretching cylinder is investigated by Naseer *et al.* [2]. Gaffar *et al.* [3] inspected the flow of a tangent hyperbolic liquid in the presence of hydrodynamic and thermal slip condition. Effect of melting heat transfer and magnetic field stagnation point flow of tangent hyperbolic liquid is examined by Hayat *et al.* [4]. Hayat *et al.* [5] studied the effects of non-linear thermal radiation and chemical reaction in the stagnation point flow of a tangent hyperbolic nanoliquid.

Development of high-energy storage technologies has been the new topic of the engineers, modelers, mathematicians and computer scientists for the past few years, because of its promising demands in various industrial and technological sectors. Heat transfer can be latently changed by varying boundary conditions, flow geometry or by upgrading the thermal conductivity of the liquid. It is a crucial challenge for researchers to enhance the heat transfer characteristics of traditional liquids like oil, ethylene glycol and water (which have low thermal conductivity). During the past few years, a new technology has been established to enhance the thermal performance. Modern technology gives new opportunities to process and produce material with average crystal size below 50 nm. In view of all this, the first attempt made by Choi [6] in this direction is to pronounce the thermal conductivity of traditional liquids inserting nanosized metallic particles. The mixture thus obtained is named nanofluid. Commonly used nanomaterials are made up of metals, *e.g.*, copper, gold, silver, etc., metallic oxides, *e.g.*, iron oxide, zinc oxide, aluminium oxide, etc., nitrides and carbides, *e.g.*, AlN, SiN, SiC, TiC, etc. Nanoparticles can also have different shapes, *e.g.*, spherical nanoparticles, disk-like

[a] e-mail: ikramu020@yahoo.com (corresponding author)

nanoparticles, rod-like nanoparticles (nanotubes), etc. In industry, nanofluids are used as coolants in the automobiles, in IT appliances and in nuclear reactors. The compilation and storage of energy through solar and geothermal means also makes use of nanofluids at the microscale level. Moreover, heat exchangers, chemical industry, processing industry, food processing, automotive, etc., have tremendous applications of the newly developed nanotechnology. Subject to such wide applications, several investigations have been carried out to analyze different aspects of nanofluids. Some of these investigations can be found in refs. [7–17]. Furthermore, magneto-nanofluids play a remarkable role in non-linear optical materials, tunable optical fiber filters, optical switches, magnetic resonance imaging (MRI), optical grating, blockage removal in the arteries, drug delivery, cancer therapy, hyperthermia, blood pump machines, magnetotherapy, arterial flows, etc. Some valuable reports in this way can be viewed in refs. [18–22] and several studies therein.

The flow generated by the stretching of a sheet is useful in many engineering and industrial processes. Consideration of liquid films, melt spinning procedures, aerodynamics, plastic sheets extrusion, production of glass fibre, the drying and cooling of textiles and paper, water pipes, irrigation channels, sewer pipes, blood vessels, food stuffs, slurries, cooling of electronic chips or metallic sheets, hot rolling, etc., are mentioned in this direction. Several engineers and scientists have discussed different issues related to flow by linear stretching. However, in the industrial and technological process, the stretching of the surface is not linear. For instance, in plastic and rubber industries the stretching process is non-linear. In particular, the non-linear stretching of surface plays a remarkable role in the polymer extrusion procedure. In view of such facts some attempts [23–28] have been made.

The prime objective of this communication is to explore the non-linear stretched magnetohydrodynamic flow of a tangent hyperbolic fluid with nanoparticles. The impacts of thermophoresis and Brownian motion are also described. Prescribed heat flux (PHF) and prescribed concentration flux (PCF) conditions are considered [29–32]. We here prefer to utilize nanoparticles in the two-dimensional non-linear stretched flow of a tangent hyperbolic liquid. A non-uniform magnetic field conducts the liquid. Boundary layer concept and assumption of weaker magnetic Reynolds number are imposed. The resulting non-linear problem is computed through the homotopic technique [33–40]. The discussion of plots and numerical computations are performed and analyzed. Surface drag coefficient and local Nusselt and Sherwood numbers are further discussed.

2 Problem statement

We explore the 2D flow of a tangent hyperbolic nanofluid. The sheet is continuously stretched with the non-linear velocity $u_w = ax^m$ (where a is a dimensional constant). A non-uniform magnetic field is implemented in the transverse direction perpendicular to the sheet. The magnetic Reynold number is selected small. The x- and y-axes are taken in the horizontal (along the stretched surface) and vertical directions, respectively. Brownian diffusion and thermophoresis effects are encountered with prescribed heat and mass flux conditions. The governing expressions for the tangent hyperbolic nanofluid can be expressed as

$$\frac{\partial u}{\partial x} + \frac{\partial v}{\partial y} = 0, \tag{1}$$

$$u\frac{\partial u}{\partial x} + v\frac{\partial u}{\partial y} = \nu(1-n)\frac{\partial^2 u}{\partial y^2} + \sqrt{2}\nu n\lambda\left(\frac{\partial u}{\partial y}\right)\frac{\partial^2 u}{\partial y^2} - \frac{\sigma B^2(x)}{\rho_f}u, \tag{2}$$

$$u\frac{\partial T}{\partial x} + v\frac{\partial T}{\partial y} = \alpha_f\frac{\partial^2 T}{\partial y^2} + \tau\left(D_B\frac{\partial T}{\partial y}\frac{\partial C}{\partial y} + \frac{D_T}{T_\infty}\left(\frac{\partial T}{\partial y}\right)^2\right), \tag{3}$$

$$u\frac{\partial C}{\partial x} + v\frac{\partial C}{\partial y} = D_B\frac{\partial^2 C}{\partial y^2} + \frac{D_T}{T_\infty}\left(\frac{\partial^2 T}{\partial y^2}\right). \tag{4}$$

The relevant conditions are

$$u = u_w(x) = ax^m, \quad v = 0, \quad -k\left(\frac{\partial T}{\partial y}\right) = q_w, \quad -D_B\left(\frac{\partial C}{\partial y}\right) = j_w \quad \text{at } y = 0, \tag{5}$$

$$u \to 0, \quad v \to 0, \quad T \to T_\infty, \quad C \to C_\infty \quad \text{as } y \to \infty. \tag{6}$$

Here u and v express the liquid velocity parallel to the x- and y-directions, respectively, m the velocity power index, μ the dynamic viscosity, ν the kinematic viscosity, ρ stands for density, $\alpha_f = \frac{k}{(\rho c)_f}$ thermal diffusivity, k indicates thermal conductivity, λ the time-dependent material parameter, τ the ratio of the heat capacity of fluid of the nanoparticles material to the effective heat capacity of the base fluid, D_B denotes the Brownian diffusion coefficient, C the nanoparticles concentration, D_T the thermophoretic diffusion, q_w the heat flux, j_w the mass flux, T_w and T_∞

are the sheet and ambient liquid temperatures and C_∞ the ambient fluid concentration. With the aid of the following variables,

$$u = ax^m f'(\eta), \qquad v = -\left(\frac{a\nu(m+1)}{2}\right)^{1/2} x^{\frac{m-1}{2}} \left(f(\eta) + \frac{m-1}{m+1}\eta f'(\eta)\right),$$
$$T = T_\infty + \sqrt{\frac{\nu}{a}}\frac{q_w}{k}\theta(\eta), \qquad C = C_\infty + \sqrt{\frac{\nu}{a}}\frac{j_w}{D_B}\phi(\eta), \qquad \eta = \left(\frac{a(m+1)}{2\nu}\right)^{1/2} x^{\frac{m-1}{2}} y, \tag{7}$$

the incompressibility condition is trivially satisfied and eqs. (2)–(6) are reduced to

$$(1-n)\left(\frac{m+1}{2}\right)f''' + \left(\frac{m+1}{2}\right)ff'' - mf'^2 + (m+1)^{\frac{3}{2}}nWef''f''' - M^2 f' = 0, \tag{8}$$
$$\theta'' + \Pr\left(f\theta' + N_b\theta'\phi' + N_t\theta'^2\right) = 0, \tag{9}$$
$$\phi'' + Le\Pr f\phi' + \frac{N_t}{N_b}\theta'' = 0, \tag{10}$$
$$f = 0, \quad f' = 1, \quad \theta' = -1, \quad \phi' = -1 \quad \text{at } \eta = 0, \tag{11}$$
$$f' \to 0, \quad \theta \to 0, \quad \phi \to 0 \quad \text{as } \eta \to \infty. \tag{12}$$

Here n designates the power-law index, We presents the Weissenberg number, Pr expresses the Prandtl number, N_b indicates the Brownian motion variable, Le is the Lewis number, N_t signifies the thermophoresis parameter and prime indicates derivative via η. These quantities are expressed as follows:

$$M^2 = \frac{2\sigma B_0^2}{a\rho_f(n+1)}, \qquad We = \frac{a^{\frac{3}{2}}x^{\frac{3m-1}{2}}\lambda}{2\sqrt{\nu}}, \qquad \Pr = \frac{\nu}{\alpha_f},$$
$$N_b = \tau\frac{D_B(C_w - C_\infty)}{\nu}, \qquad N_t = \tau\frac{D_T(T_w - T_\infty)}{\nu T_\infty}, \qquad Le = \frac{\alpha_f}{D_B}. \tag{13}$$

The surface drag coefficient is expressed as follows:

$$C_f = \frac{2\tau_w}{\rho_f u_w^2}, \qquad \tau_w = \mu\left[(1-n)\frac{\partial u}{\partial y} + \frac{n\lambda}{\sqrt{2}}\left(\frac{\partial u}{\partial y}\right)^2\right]. \tag{14}$$

In non-dimensional form we have

$$\sqrt{\mathrm{Re}}C_f = \left[(1+m)(1-n)f''(\eta) + \frac{n}{2}(1+m)We\left(f''(\eta)\right)^2\right]_{\eta=0}. \tag{15}$$

The surface heat and mass transfer rates in dimensionless form can be put into the definitions

$$(\mathrm{Re})^{-0.5}Nu_x = \frac{1}{\theta(0)}, \qquad (\mathrm{Re})^{-0.5}Sh_x = \frac{1}{\phi(0)}, \tag{16}$$

where the local Reynolds number is denoted by $\mathrm{Re}_x = u_w x/\nu$.

3 Series expressions

The initial estimates and operators regarding homotopic procedures are:

$$f_0(\eta) = 1 - e^{-\eta}, \qquad \theta_0(\eta) = e^{-\eta}, \qquad \phi_0(\eta) = e^{-\eta}, \tag{17}$$
$$\bar{\mathcal{L}}_1 = f''' - f', \qquad \bar{\mathcal{L}}_2 = \theta'' - \theta, \qquad \bar{\mathcal{L}}_3 = \phi'' - \phi, \tag{18}$$
$$\left.\begin{aligned} &\bar{\mathcal{L}}_1\left[c_1^{**} + c_2^{**}e^{\eta} + c_3^{**}e^{-\eta}\right] = 0,\\ &\bar{\mathcal{L}}_2\left[c_4^{**}e^{\eta} + c_5^{**}e^{-\eta}\right] = 0,\\ &\bar{\mathcal{L}}_3\left[c_6^{**}e^{\eta} + c_7^{**}e^{-\eta}\right] = 0, \end{aligned}\right\}, \tag{19}$$

in which c_i^{**} $(i = 1\text{–}7)$ designates the constants.

The statements of zero-th order are

$$(1-\breve{p})\bar{\mathcal{L}}_1\left[\hat{f}(\eta,\breve{p})-f_0(\eta)\right]=\breve{p}\hbar_f\mathcal{N}_f\left[\hat{f}(\eta,\breve{p})\right], \tag{20}$$

$$(1-\breve{p})\bar{\mathcal{L}}_2\left[\hat{\theta}(\eta,\breve{p})-\theta_0(\eta)\right]=\breve{p}\hbar_\theta\mathcal{N}_\theta\left[\hat{f}(\eta,\breve{p}),\hat{\theta}(\eta,\breve{p}),\hat{\phi}(\eta,\breve{p})\right], \tag{21}$$

$$(1-\breve{p})\bar{\mathcal{L}}_3\left[\hat{\phi}(\eta,\breve{p})-\phi_0(\eta)\right]=\breve{p}\hbar_\phi\mathcal{N}_\phi\left[\hat{f}(\eta,\breve{p}),\hat{\theta}(\eta,\breve{p}),\hat{\phi}(\eta,\breve{p})\right], \tag{22}$$

$$\left.\begin{aligned}&\hat{f}(0,\breve{p})=0,\qquad \hat{f}'(0,\breve{p})=1,\qquad \hat{f}'(\infty,\breve{p})=0,\qquad \hat{\theta}'(0,\breve{p})=-1,\\&\hat{\theta}(\infty,\breve{p})=0,\qquad \hat{\phi}'(0,\breve{p})=-1,\qquad \hat{\phi}(\infty,\breve{p})=0,\end{aligned}\right\} \tag{23}$$

$$\mathcal{N}_f\left[\hat{f}(\eta;\breve{p})\right]=\left(\frac{m+1}{2}\right)(1-n)\frac{\partial^3\hat{f}}{\partial\eta^3}+\left(\frac{m+1}{2}\right)\hat{f}\frac{\partial^2\hat{f}}{\partial\eta^2}-m\left(\frac{\partial\hat{f}}{\partial\eta}\right)^2+(m+1)^{\frac{3}{2}}nWe\frac{\partial^2\hat{f}}{\partial\eta^2}\frac{\partial^3\hat{f}}{\partial\eta^3}-M^2\frac{\partial\hat{f}}{\partial\eta}, \tag{24}$$

$$\mathcal{N}_\theta\left[\hat{\theta}(\eta,\breve{p}),\hat{\phi}(\eta,\breve{p}),\hat{f}(\eta;\breve{p})\right]=\frac{\partial^2\hat{\theta}}{\partial\eta^2}+\Pr\hat{f}\frac{\partial\hat{\theta}}{\partial\eta}+\Pr N_b\frac{\partial\hat{\theta}}{\partial\eta}\frac{\partial\hat{\phi}}{\partial\eta}+\Pr N_t\left(\frac{\partial\hat{\theta}}{\partial\eta}\right)^2, \tag{25}$$

$$\mathcal{N}_\phi\left[\hat{\phi}(\eta,\breve{p}),\hat{\theta}(\eta,\breve{p}),\hat{f}(\eta;\breve{p})\right]=\frac{\partial^2\hat{\phi}}{\partial\eta^2}+Le\Pr\hat{f}\frac{\partial\hat{\phi}}{\partial\eta}+\frac{N_t}{N_b}\frac{\partial^2\hat{\theta}}{\partial\eta^2}. \tag{26}$$

Here $\breve{p}$ designates the embedding variable, ($\hbar_f$, $\hbar_\theta$ and $\hbar_\phi$) the auxiliary variables and ($\mathcal{N}_f$, $\mathcal{N}_\theta$ and $\mathcal{N}_\phi$) the non-linear operators. Now $\breve{p}=0$ and $\breve{p}=1$ lead to

$$\begin{aligned}&\hat{f}(\eta;0)=f_0(\eta),\qquad \hat{\theta}(\eta,0)=\theta_0(\eta),\qquad \hat{\phi}(\eta,0)=\phi_0(\eta),\\&\hat{f}(\eta;1)=f(\eta),\qquad \hat{\theta}(\eta,1)=\theta(\eta),\qquad \hat{\phi}(\eta,1)=\phi(\eta).\end{aligned} \tag{27}$$

When $\breve{p}$ moves from 0 towards 1 then ($\hat{f}(\eta;\breve{p})$, $\hat{\theta}(\eta,\breve{p})$ and $\hat{\phi}(\eta,\breve{p})$) change from the initial estimations ($f_0(\eta)$, $\theta_0(\eta)$ and $\phi_0(\eta)$) to expressions ($f(\eta)$, $\theta(\eta)$ and $\phi(\eta)$), respectively. Considering

$$\hat{f}(\eta;\breve{p})=f_0(\eta)+\sum_{m=1}^{\infty}f_m(\eta)\breve{p}^m,\qquad f_m(\eta)=\left.\frac{1}{m!}\frac{\partial^m\hat{f}(\eta,\breve{p})}{\partial\breve{p}^m}\right|_{\breve{p}=0}, \tag{28}$$

$$\hat{\theta}(\eta;\breve{p})=\theta_0(\eta)+\sum_{m=1}^{\infty}\theta_m(\eta)\breve{p}^m,\qquad \theta_m(\eta)=\left.\frac{1}{m!}\frac{\partial^m\hat{\theta}(\eta,\breve{p})}{\partial\breve{p}^m}\right|_{\breve{p}=0}, \tag{29}$$

$$\hat{\phi}(\eta;\breve{p})=\phi_0(\eta)+\sum_{m=1}^{\infty}\phi_m(\eta)\breve{p}^m,\qquad \phi_m(\eta)=\left.\frac{1}{m!}\frac{\partial^m\hat{\phi}(\eta,\breve{p})}{\partial\breve{p}^m}\right|_{\breve{p}=0} \tag{30}$$

and ($\hbar_f$, $\hbar_\theta$ and $\hbar_\phi$), in such a fashion that eqs. (28)–(30) converge for $\breve{p}=1$, then we have

$$\hat{f}(\eta)=f_0(\eta)+\sum_{m=1}^{\infty}f_m(\eta), \tag{31}$$

$$\hat{\theta}(\eta)=\theta_0(\eta)+\sum_{m=1}^{\infty}\theta_m(\eta), \tag{32}$$

$$\hat{\phi}(\eta)=\phi_0(\eta)+\sum_{m=1}^{\infty}\phi_m(\eta). \tag{33}$$

The m-th–order problems are

$$\bar{\mathcal{L}}_1\left[f_m(\eta)-\chi_m f_{m-1}(\eta)\right]=\hbar_f\check{\mathcal{R}}_f^m(\eta), \tag{34}$$

$$\bar{\mathcal{L}}_2\left[\theta_m(\eta)-\chi_m\theta_{m-1}(\eta)\right]=\hbar_\theta\check{\mathcal{R}}_\theta^m(\eta), \tag{35}$$

$$\bar{\mathcal{L}}_3\left[\phi_m(\eta)-\chi_m\phi_{m-1}(\eta)\right]=\hbar_\phi\check{\mathcal{R}}_\phi^m(\eta), \tag{36}$$

$$\left.f_m(0)=f_m'(0)=f_m'(\infty)=0,\qquad \theta_m'(0)=\theta_m(\infty)=0,\phi_m'(0)=\phi_m(\infty)=0,\right\} \tag{37}$$

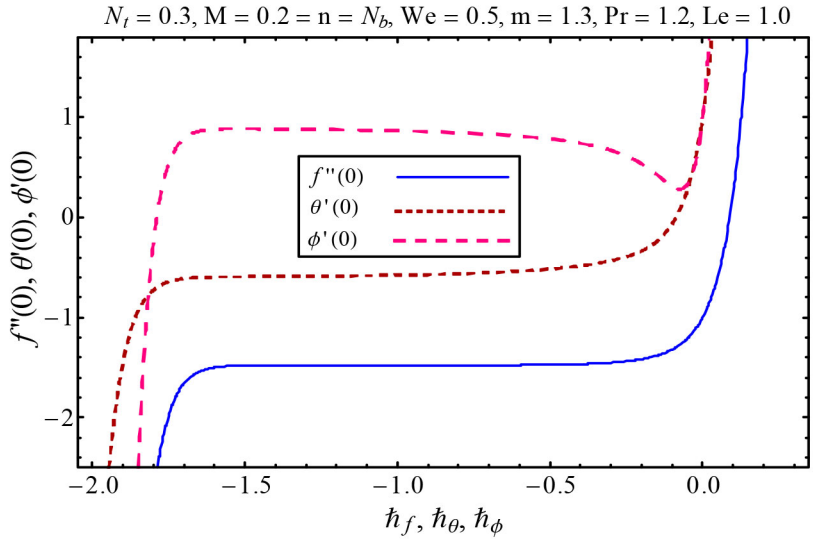

Fig. 1. The $\hbar$-curves for $f(\eta)$, $\theta(\eta)$ and $\phi(\eta)$.

$$\check{\mathcal{R}}_f^m(\eta) = \left(\frac{m+1}{2}\right)(1-n)f'''_{m-1}(\eta) + \left(\frac{m+1}{2}\right)\sum_{k=0}^{m-1} f_{m-1-k}f''_k - m\sum_{k=0}^{m-1} f'_{m-1-k}f'_k + (m+1)^{\frac{3}{2}}nWe\sum_{k=0}^{m-1} f''_{m-1-k}f'''_k - M^2 f'_{m-1}(\eta), \tag{38}$$

$$\check{\mathcal{R}}_\theta^m(\eta) = \theta''_{m-1}(\eta) + \Pr\sum_{k=0}^{m-1} f_{m-1-k}\theta'_k + \Pr N_b\sum_{k=0}^{m-1}\phi'_{m-1-k}\theta'_k + \Pr N_t\sum_{k=0}^{m-1}\theta'_{m-1-k}\theta'_k, \tag{39}$$

$$\check{\mathcal{R}}_\phi^m(\eta) = \phi''_{m-1}(\eta) + Le\Pr\sum_{k=0}^{m-1} f_{m-1-k}\phi'_k + \left(\frac{N_t}{N_b}\right)\theta''_{m-1}(\eta), \tag{40}$$

$$\chi_m = \begin{cases} 0, & m \le 1, \\ 1, & m > 1. \end{cases} \tag{41}$$

The general solutions for the governing equations are expressed as follows:

$$f_m(\eta) = f_m^*(\eta) + c_1^{**} + c_2^{**}e^{\eta} + c_3^{**}e^{-\eta}, \tag{42}$$

$$\theta_m(\eta) = \theta_m^*(\eta) + c_4^{**}e^{\eta} + c_5^{**}e^{-\eta}, \tag{43}$$

$$\phi_m(\eta) = \phi_m^*(\eta) + c_6^{**}e^{\eta} + c_7^{**}e^{-\eta}, \tag{44}$$

where special solutions are presented by $f_m^*(\eta)$, $\theta_m^*(\eta)$ and $\phi_m^*(\eta)$.

4 Convergence analysis

It is a well-known fact that the convergence of (31)–(33) strongly depends upon the auxiliary parameters $\hbar_f$, $\hbar_\theta$ and $\hbar_\phi$. The region of convergence and rate of estimations for the functions f, θ and ϕ can be adjusted and controlled via these auxiliary variables. To determine the acceptable ranges of these variables, we interpreted $\hbar$-curves at the 19-th order of deformations (see fig. 1). Figure 1 shows that the acceptable ranges of $\hbar_f$, $\hbar_\theta$ and $\hbar_\phi$ are $-1.6 \le \hbar_f \le -0.6$, $-1.7 \le \hbar_\theta \le -0.5$ and $-1.6 \le \hbar_\phi \le -0.6$. Furthermore, the presented series solutions are convergent in all zones of η, when $\hbar_f = -1.0$ and $\hbar_\theta = -1.0 = \hbar_\phi$. Table 1 is drawn to show how many order of estimations are adequate for the convergent solutions. This table clearly demonstrates that the 25th and the 50th orders of estimations are adequate for the convergence of f, θ and ϕ.

Table 1. Homotopic convergence solutions when $M = n = 0.2 = N_b$, $N_t = 0.3$, $We = 0.5$, Pr $= 1.2$, $Le = 1.0$, $m = 1.3$.

Order of estimations	$-f''(0)$	$-\theta''(0)$	$\phi''(0)$
1	1.3013	0.1000	0.4500
5	1.4528	0.4302	0.6702
10	1.4741	0.5275	0.8006
15	1.4775	0.5625	0.8475
25	1.4784	0.5872	0.8813
35	1.4784	0.5949	0.8924
45	1.4784	0.5978	0.8966
50	1.4784	0.5985	89776
55	1.4784	0.5985	89776

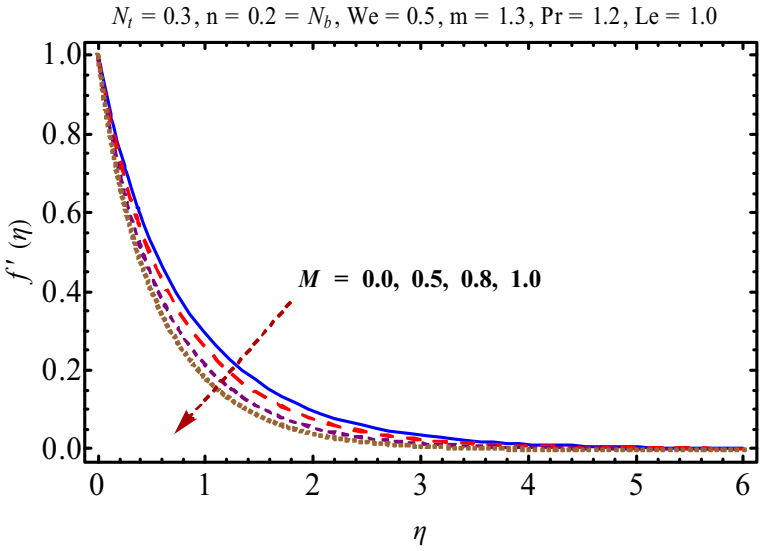

Fig. 2. Variation of $f'(\eta)$ via M.

5 Discussion and results

The main focus of the current section is to report the consequences of velocity $f'(\eta)$, temperature $\theta(\eta)$ and concentration $\phi(\eta)$ distributions corresponding to distinct values of emerging variables, like magnetic parameter M, Prandtl number Pr, velocity index m, Brownian motion parameter N_b, Weissenberg number We, power-law index n, thermophoresis parameter N_t and Lewis number Le. For such analysis, figs. 2–17 are interpreted. Figure 2 displays variations in velocity field for numerous values of magnetic variable M. We infer, from this figure, that a larger magnetic parameter reduces the fluid velocity. Physically, the applied magnetic field has the characteristic of slowing down the liquid and, consequently, reducing liquid velocity. Figure 3 shows the characteristics of the Weissenberg number We for the velocity field $f'(\eta)$. It is observed that $f'(\eta)$ decreases when We is enhanced. Figure 4 provides the description for results of velocity index m on velocity $f'(\eta)$. Clearly the fluid velocity diminishes by velocity index m. It is due to the fact that an inflation in m reduces the stretching rate and ultimately it slows down fluid velocity and reduces the momentum layer thickness. The effect of power-law index n on velocity field $f'(\eta)$ is displayed in fig. 5. Here we declare that higher values of n lead to decaying in fluid velocity. Figure 6 shows the magnetic parameter effect on the temperature field. Thermal layer decays by enhancing magnetic parameter. In fact, magnetic variable relies on the Lorentz force. Higher M has strong Lorentz force which resists the fluid motion and thus makes the fluid temperature increase. For $M = 0$, the flow is hydrodynamic whereas, for $M > 0$, it corresponds to a hydromagnetic case.

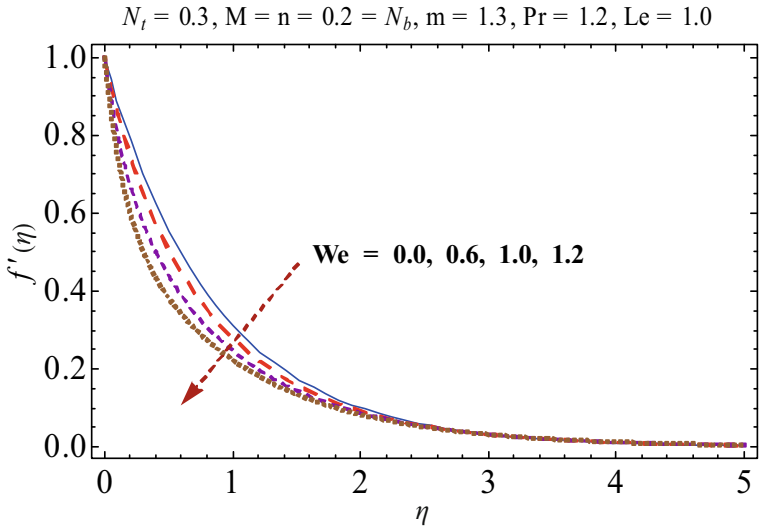

Fig. 3. Variation of $f'(\eta)$ via We.

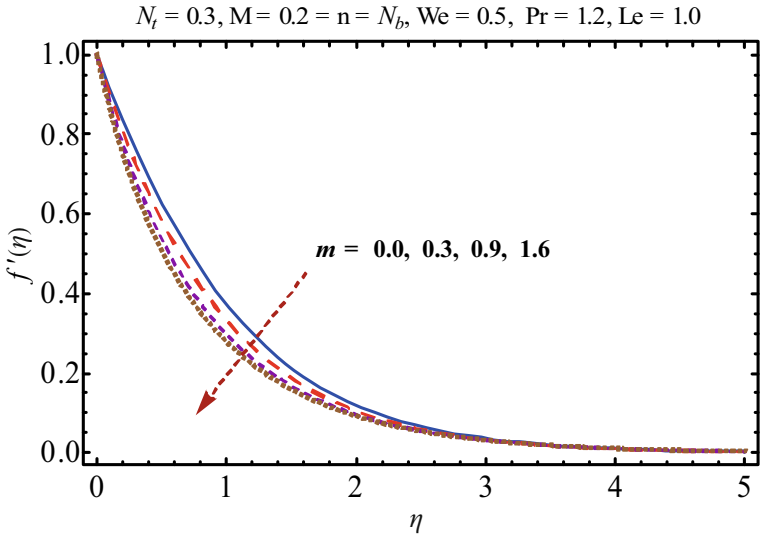

Fig. 4. Variation of $f'(\eta)$ via m.

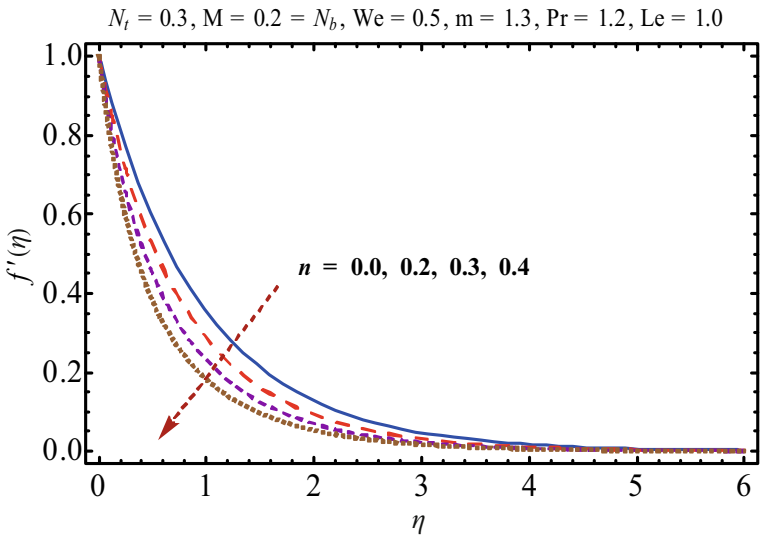

Fig. 5. Variation of $f'(\eta)$ via n.

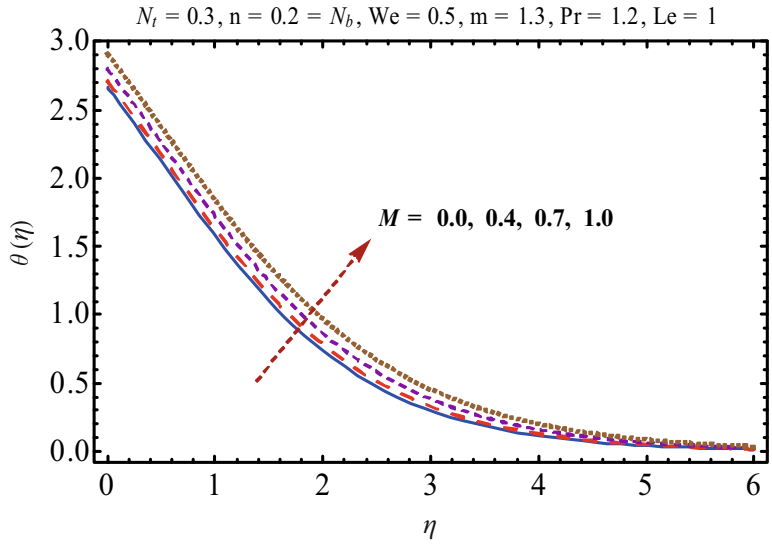

Fig. 6. Variation of $\theta(\eta)$ via M.

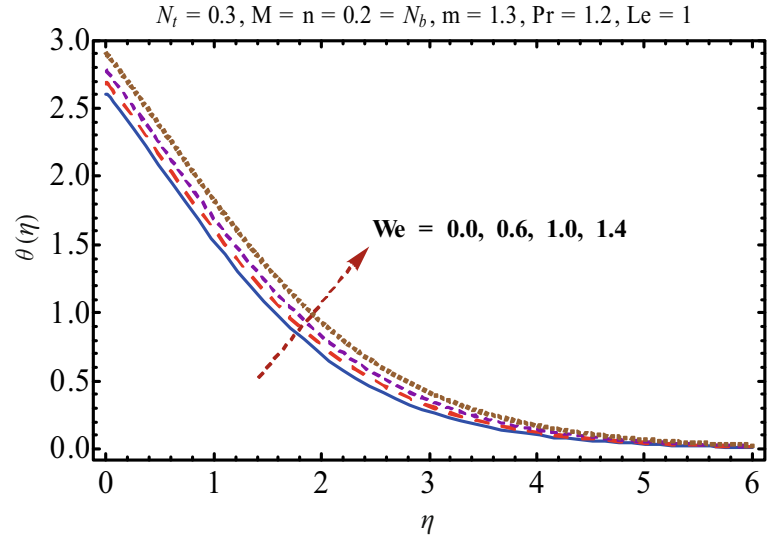

Fig. 7. Variation of $\theta(\eta)$ via We.

Influence of Weissenberg number We on temperature $\theta(\eta)$ is analyzed in fig. 7. Fluid temperature is found to increase via We. Weissenberg is the relaxation time of the liquid and the specific time process ratio. With the increment in We, the relaxation time enhances, which puts forward more opposition to the liquid motion and, thus, it makes the fluid temperature rise. Figure 8 exhibits the consequences of temperature $\theta(\eta)$ *versus* n. Here temperature is an increasing function of n. Variations in the Prandtl number Pr on $\theta(\eta)$ is presented in fig. 9. Higher Pr fluid corresponds to lower thermal diffusivity. Such difference in thermal diffusivity corresponds to decay in liquid temperature. Figure 10 shows the effects of velocity index m on temperature field. Obviously, temperature profile $\theta(\eta)$ is enhanced by increasing m. Higher values of m restrict the stretching rate due to which less number of hot particles moves from surface to the ambient fluid thereby fluid temperature blows up. Figure 11 displays the effects of thermophoresis variable N_t on $\theta(\eta)$. The more effective thermophoretic force permits nanoparticles of high thermal conductivity deeper into the liquid, which results in an increase in the liquid temperature. In fig. 12, the temperature distribution enhances via Brownian motion variable N_b. Increment in N_b enhances the collision between the particles, which produces more heat and ultimately the temperature enhances. Impact of velocity index m on $\phi(\eta)$ is plotted in fig. 13. It is evident that larger m suppresses the concentration of fluid. Variations in We give rise to liquid concentration (see fig. 14).

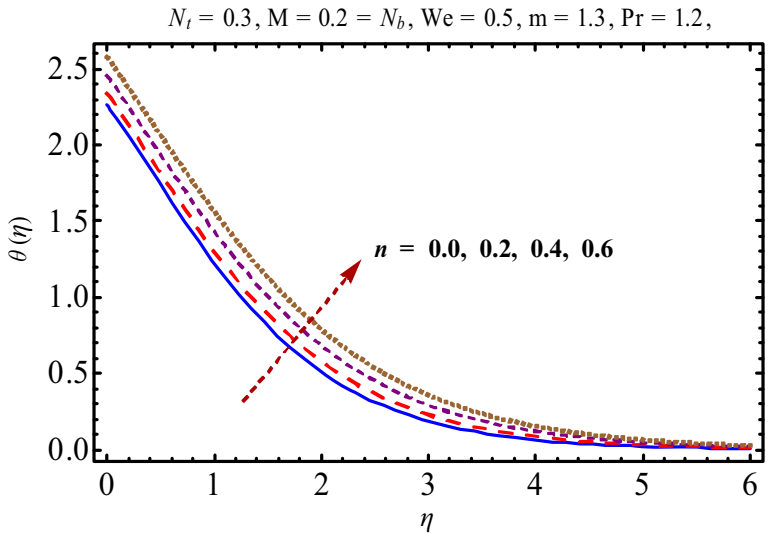

Fig. 8. Variation of $\theta(\eta)$ via n.

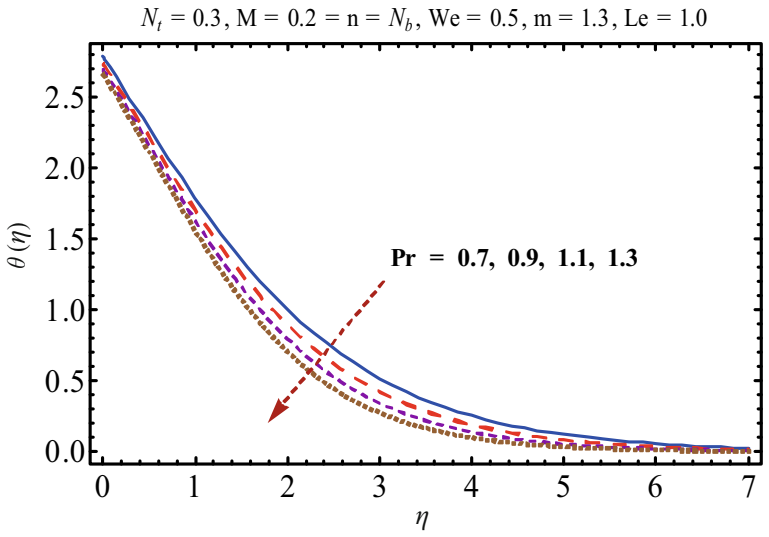

Fig. 9. Variation of $\theta(\eta)$ via Pr.

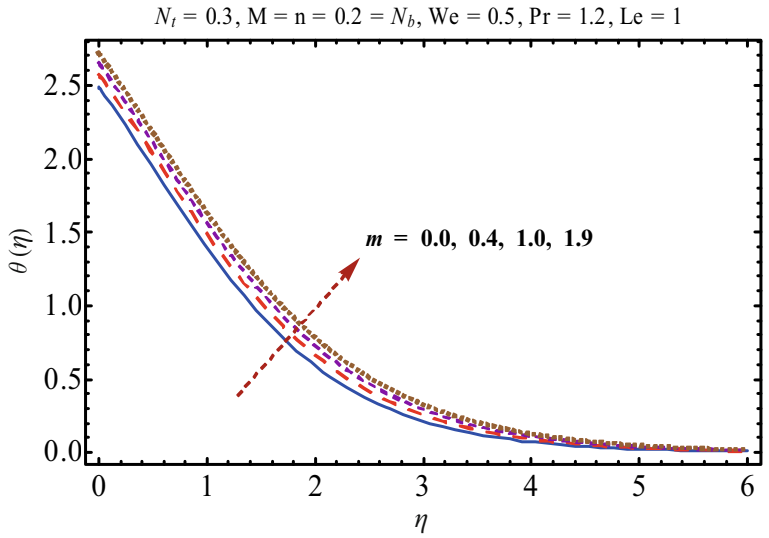

Fig. 10. Variation of $\theta(\eta)$ via m.

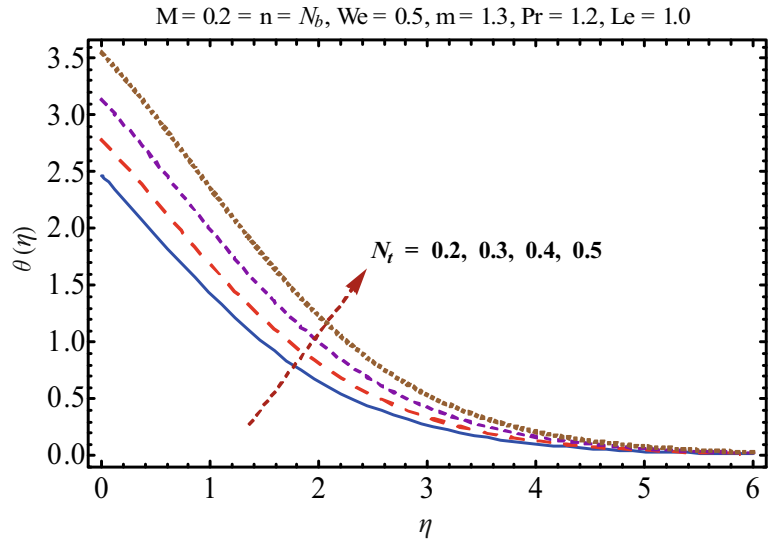

Fig. 11. Variation of $\theta(\eta)$ via N_t.

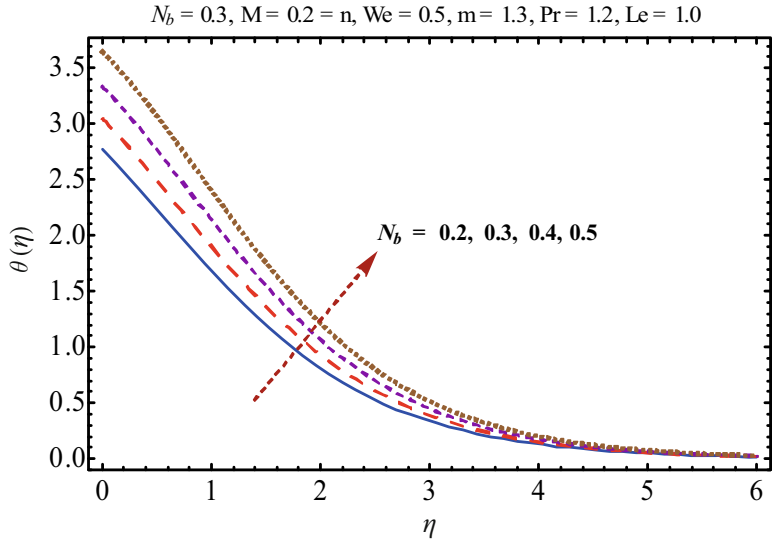

Fig. 12. Variation of $\theta(\eta)$ via N_b.

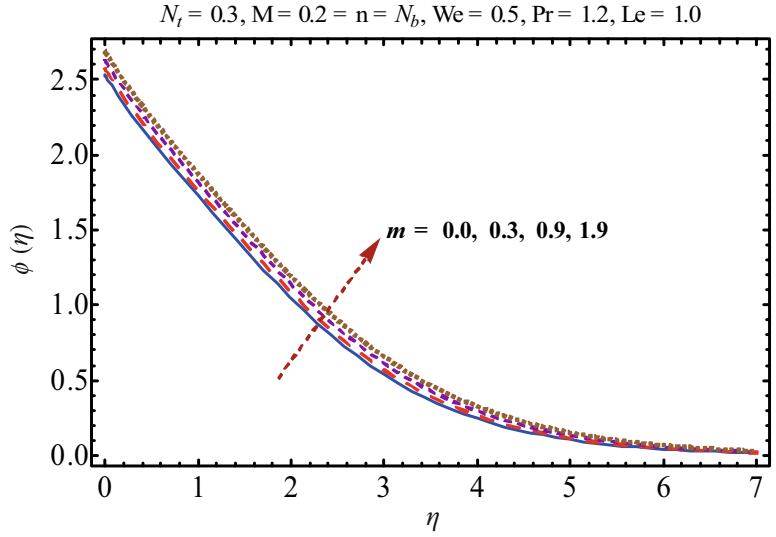

Fig. 13. Variation of $\phi(\eta)$ via N_t.

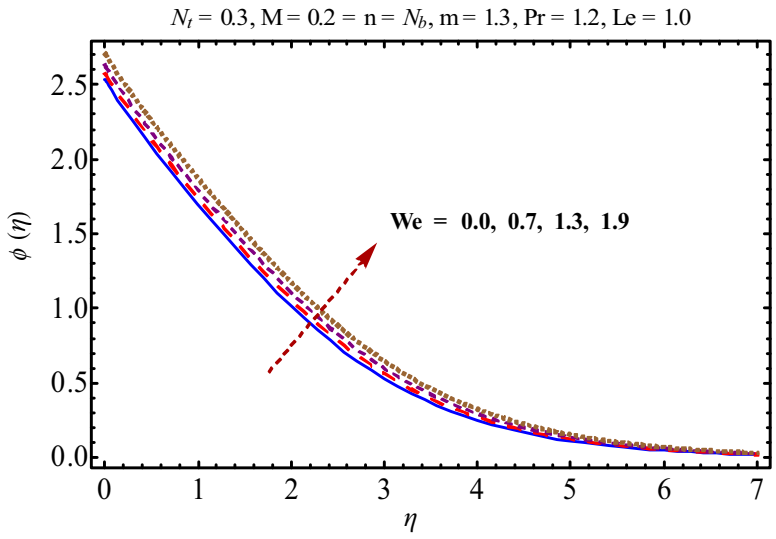

Fig. 14. Variation of $\phi(\eta)$ via We.

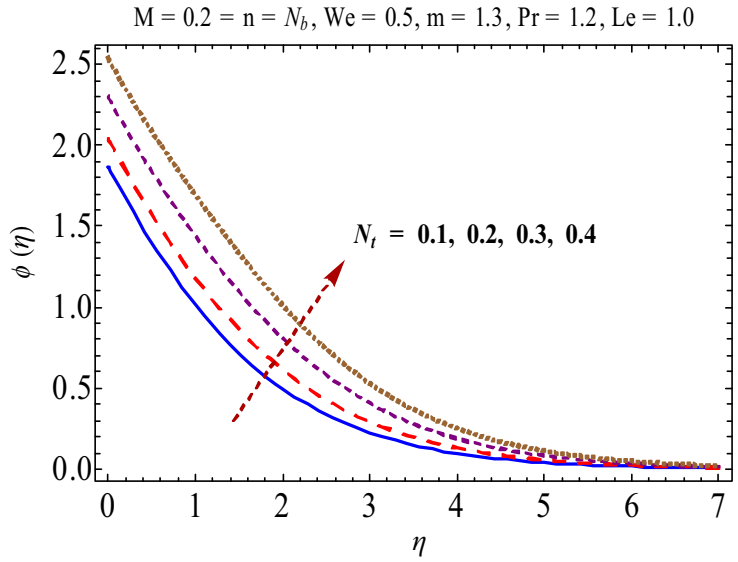

Fig. 15. Variation of $\phi(\eta)$ via N_t.

Figure 15 shows the behavior of N_t on the concentration profile. Larger values of N_t blow up the concentration and corresponding concentration layer thickness. Figure 16 displays the feature of Brownian motion variable N_b on $\phi(\eta)$. It is concluded that an increase in N_b is responsible for a reduction in the fluid concentration. Figure 17 provides Lewis number Le characteristics on concentration field. The concentration layer decays by enhancing Le. In fact, an increment in the Lewis number Le yields a decay in coefficient of Brownian diffusion which finally results in a decrease in concentration field. Figure 18 shows the effects of M on Nusselt number $(\mathrm{Re})^{-0.5}Nu_x$ via Pr. It is concluded that surface heat transfer rate enhances for higher M and Pr. Figure 19 shows the variation of N_b on $(\mathrm{Re})^{-0.5}Nu_x$ via N_t. It is observed that $(\mathrm{Re})^{-0.5}Nu_x$ increases for larger N_t while it reduces when N_b is enhanced. Figure 20 displays the effects of the velocity index m on $(\mathrm{Re})^{-0.5}Sh_x$ via Le. Here enhancement in $(\mathrm{Re})^{-0.5}Sh_x$ is noted for higher Le whereas it decreases for velocity index. Influence of magnetic parameter M on $(\mathrm{Re})^{-0.5}Sh_x$ via Lewis number is depicted in fig. 21. Here the mass transfer rate is enhanced for M and Le. Table 1 is drawn to visualize the convergence of $-f''(0)$, $-\theta''(0)$ and $\phi''(0)$ at different orders of estimations. This table portrays that the 50th order of deformations is adequate regarding the convergent analysis. It is also noted that we have to compute less number of approximations for velocity in comparison to temperature and concentration. Numerical data of skin friction coefficient is prepared in table 2. It is observed that surface drag coefficient enhances via M, We and m. Table 3 shows an excellent agreement of skin friction coefficient in the absence of both Weissenberg number and power-law index [1, 41].

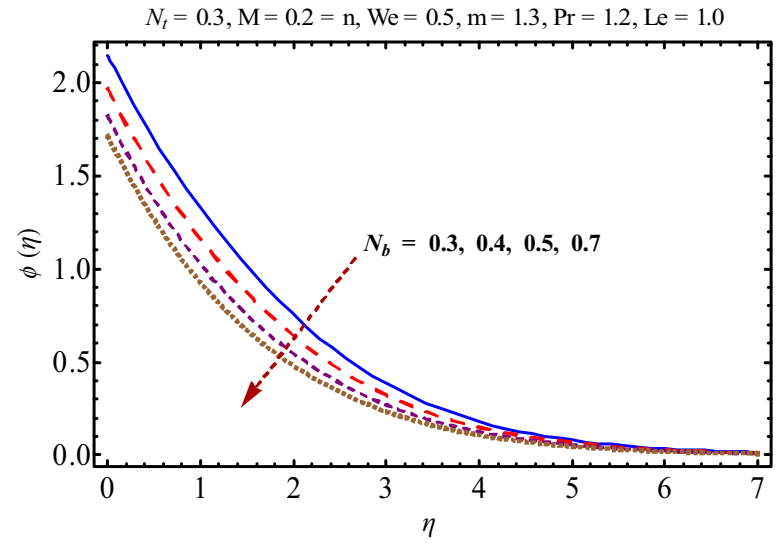

Fig. 16. Variation of $\phi(\eta)$ via N_b.

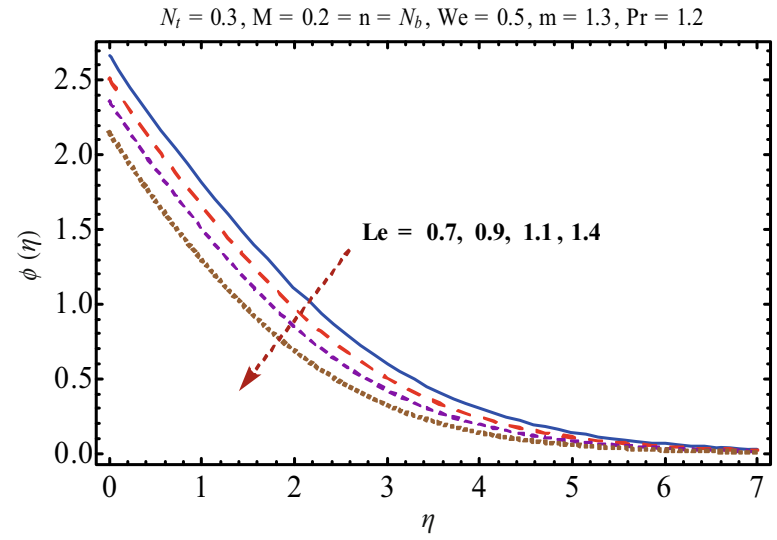

Fig. 17. Variation of $\phi(\eta)$ via Le.

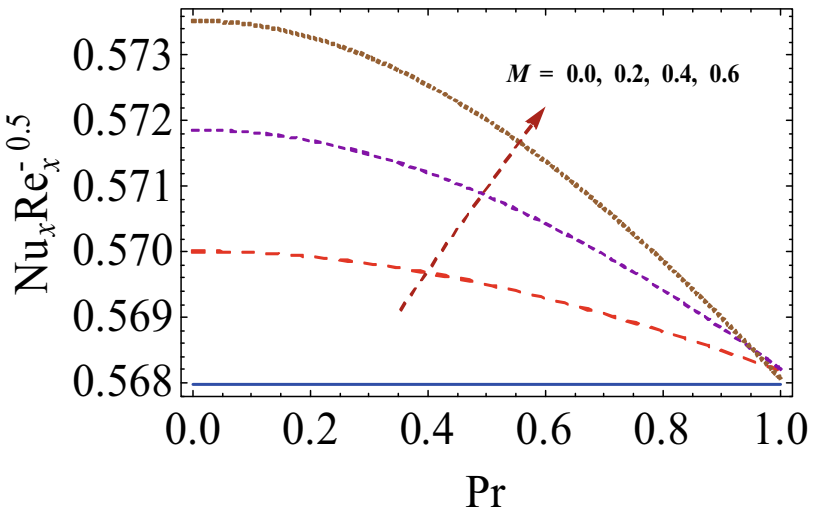

Fig. 18. Variation of M via Le on $Nu_x\,\mathrm{Re}_x^{0.5}$.

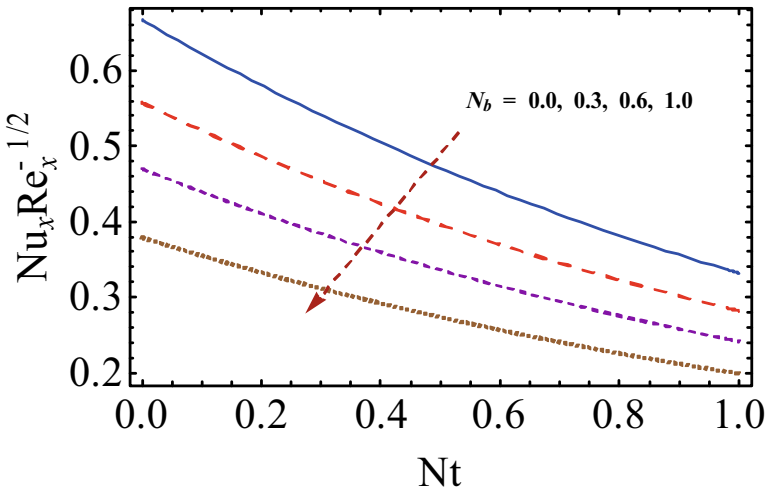

Fig. 19. Variation of N_b via N_t on $Nu_x\,\mathrm{Re}_x^{0.5}$.

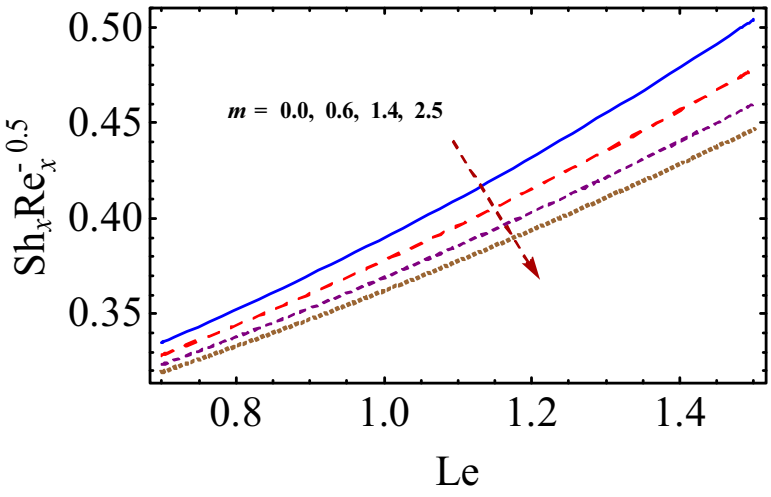

Fig. 20. Variation of m via Le on $Sh_x\,\mathrm{Re}_x^{0.5}$.

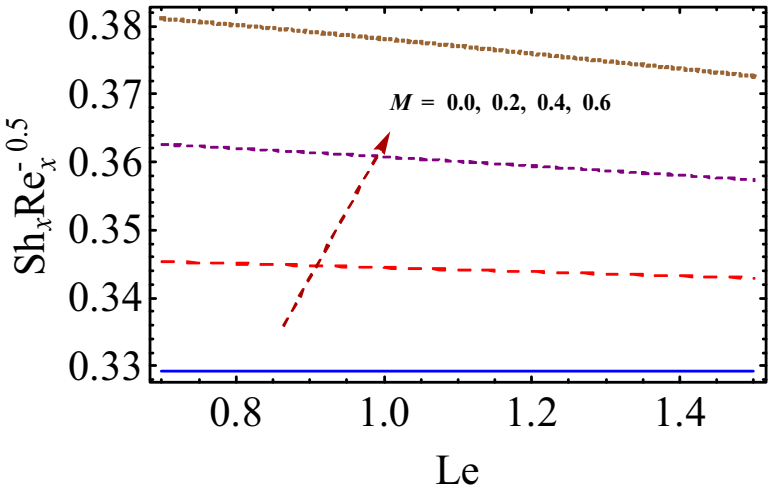

Fig. 21. Variation of M via Le on $Sh_x\,\mathrm{Re}_x^{0.5}$.

Table 2. Computation showing $(\mathrm{Re})^{1/2}C_f$ for numerous values of M, n, m and We when $N_b = 0.2$, $N_t = 0.3$, $\mathrm{Pr} = 1.2$, $Le = 1.0$.

Parameters (constant values)	Parameters		$-\mathrm{Re}^{0.5}\,C_{f_x}$
$We = 0.5$, $n = 0.2$, $m = 1.3$	M	0.0	1.4191
		0.2	1.4687
		0.4	1.6166
$n = 0.2$, $m = 1.3$, $M = 0.2$	We	0.2	1.2936
		0.4	1.4209
		0.5	1.5305
$We = 0.5$, $n = 0.2$, $M = 0.2$	m	0.0	0.3213
		1.0	1.0665
		1.5	1.8610
$We = 0.5$, $m = 1.3$, $M = 0.2$	n	0.1	1.4376
		0.2	1.5296
		0.3	1.9936

Table 3. Comparison of surface drag coefficient for different techniques.

Present results when	$m = 1$, $We = n = 0$	[1]	[41]
M	HAM	Numerically	Exact solution
0	1	1	
0.3	−1.04403		
0.5	−1.11803	−1.11803	−1.1180
0.8	−1.28062		
1.0	−1.41588	−1.41421	

6 Final results

Here we inspected the magnetohydrodynamic (MHD) flow of tangent hyperbolic nanoliquid over a non-linear stretched sheet with prescribed heat and mass flux conditions. Significant observations of current analysis are given as follows:

- Influences of m and M on $f'(\eta)$ and $\theta(\eta)$ distributions are quite opposite.
- Temperature field is increasing function of N_t and N_b.
- Larger values of N_t give rise to concentration profile.
- Impact of We on $\theta(\eta)$ and $\phi(\eta)$ is opposite to that of $f'(\eta)$.
- Surface drag coefficient enhances via We, M and n.
- Heat transfer rate is an increasing function of magnetic parameter.

References

1. M.A. Abbas, Y.Q. Bai, M.M. Bhatti, M.M. Rashidi, Alex. Eng. J. **55**, 653 (2016).
2. M. Naseer, M.Y. Malik, S. Nadeem, A. Rehman, Alex. Eng. J. **53**, 747 (2014).
3. S.A. Gaffar, V.R. Prasad, E.K. Reddy, O.A. Bég, Arab. J. Sci. Eng. **39**, 8157 (2014).
4. T. Hayat, A. Shafiq, A. Alsaedi, J. Magn. & Magn. Mater. **405**, 97 (2016).
5. T. Hayat, S. Qayyum, A. Alsaedi, S.A. Shehzad, J. Mol. Liq. **223**, 969 (2016).
6. S.U.S. Choi, *Enhancing thermal conductivity of fluids with nanoparticles in developments and applications of Non-Newtonian flows*, FED 231/MD 66 (1995) pp. 99–105.
7. J. Buongiorno, ASME J. Heat Transf. **128**, 240 (2006).
8. R.K. Tiwari, M.K. Das, Int. J. Heat Mass Transfer **50**, 2002 (2007).
9. K.L. Hsiao, Comput. Fluids **104**, 1 (2014).
10. A.V. Kuznetsov, D.A. Nield, Int. J. Thermal Sci. **77**, 126 (2014).
11. A. Malvandi, D.D. Ganji, J. Magn. & Magn. Mater. **362**, 172 (2014).
12. B.J. Gireesha, R.S.R. Gorla, B. Mahanthesh, J. Nanofluids **4**, 474 (2015).
13. R. Ellahi, M. Hassan, A. Zeeshan, Int. J. Heat Mass Transfer **81**, 449 (2015).
14. M. Turkyilmazoglu, Energy Convers. Manag. **114**, 1 (2016).
15. M. Sheikholeslami, M.T. Mustafa, D.D. Ganji, Particuology **26**, 108 (2016).
16. T. Hayat, I. Ullah, T. Muhammad, A. Alsaedi, J. Mol. Liq. **220**, 1004 (2016).
17. T. Hayat, M. Waqas, S.A. Shehzad, A. Alsaedi, J. Mol. Liq. **215**, 704 (2016).
18. M. Turkyilmazoglu, Comput. Fluids **71**, 426 (2013).
19. S. Rashidi, M. Dehghan, R. Ellahi, M. Riaz, M.T. Jamal-Abad, J. Magn. & Magn. Mater. **378**, 128 (2015).
20. C. Zhang, L. Zheng, X. Zhang, G. Chen, Appl. Math. Model **39**, 165 (2015).
21. T. Hayat, M. Imtiaz, A. Alsaedi, M.A. Kutbi, J. Magn. & Magn. Mater. **396**, 31 (2015).
22. W.A. Khan, O.D. Makinde, Z.H. Khan, Int. J. Heat Mass Transfer **96**, 525 (2016).
23. K. Vajravelu, Appl. Math. Comput. **124**, 281 (2001).
24. R. Cortell, Phys. Lett. A **372**, 631 (2008).
25. P. Rana, R. Bhargava, Commun. Nonlinear Sci. Numer. Simulat. **17**, 212 (2012).
26. S. Mukhopadhyay, Alex. Eng. J. **52**, 563 (2013).
27. F. Mabood, W.A. Khan, A.I.M. Ismail, J. Magn. & Magn. Mater. **374**, 569 (2015).
28. T. Hayat, A. Aziz, T. Muhammad, B. Ahmad, J. Magn. & Magn. Mater. **408**, 99 (2016).
29. N.A. Yacob, A. Ishak, Chem. Eng. Res. Des. **89**, 2291 (2011).
30. I.C. Mandal, S. Mukhopadhyay, Ain Shams Eng. J. **4**, 103 (2013).
31. T. Hayat, I. Ullah, T. Muhammad, A. Alsaedi, S.A. Shehzad, Chin. Phys. B **25**, 074701 (2016).
32. T. Hayat, Z. Hussain, A. Alsaedi, T. Muhammad, Neural. Comput. Appl. (2016) DOI: 10.1007/s00521-016-2685-x.
33. S. Liao, *Beyond Perturbation: Introduction to the Homotopy Analysis Method* (CRC Press, 2003).
34. T. Hayat, R. Ellahi, P.D. Ariel, S. Asghar, Nonlinear Dyn. **45**, 55 (2006).
35. M. Turkyilmazoglu, Commun. Nonlinear Sci. Numer. Simulat. **17**, 4097 (2012).
36. S. Abbasbandy, M.S. Hashemi, I. Hashim, Quaest. Math. **36**, 93 (2013).
37. T. Hayat, A. Naseem, M. Farooq, A. Alsaedi, Eur. Phys. J. Plus **128**, 158 (2013).
38. A. Qayyum, T. Hayat, M.S. Alhuthali, H.M. Malaikah, Chin. Phys. B **23**, 054703 (2014).
39. T. Hayat, S. Asad, M. Mustafa, A. Alsaedi, Comput. Fluids **108**, 179 (2015).
40. T. Hayat, M. Waqas, M.I. Khan, A. Alsaedi, Int. J. Heat Mass Transfer **102**, 1123 (2016).
41. T. Fang, J. Zhang, S. Yao, Commun. Nonlinear Sci. Numer. Simulat. **14**, 3731 (2009).